Molecular Composition and Orientation in Myelin Figures Characterized by Coherent Anti-Stokes Raman Scattering Microscopy

Alan P. Kennedy, Jonathan Sutcliffe, and Ji-Xin Cheng*

Weldon School of Biomedical Engineering and Department of Chemistry, Purdue University, West Lafayette, Indiana 47907

Received December 21, 2004. In Final Form: April 18, 2005

The molecular organization inside myelin figures of various surfactants are studied by laser scanning coherent anti-Stokes Raman scattering (CARS) microscopy that permits three-dimension vibrational imaging. The resonant CARS signals from CH_2 and H_2O stretch vibrations are used to probe the surfactant and water molecules inside the myelin figures formed of $C_{12}E_3$, lecithin, and Aerosol OT. The polarization sensitivity of CARS is used to analyze the orientation of the CH_2 groups and the H_2O molecules. The CARS images suggest that the myelin figure is a concentric lamellar structure with alternating surfactant bilayers and partially ordered water layers. No sizable water core is observed in the CARS images at the lateral resolution of 0.3 μm and the axial resolution of 0.75 μm. The CARS data are verified by confocal fluorescence microscopy with FITC and DOPE−rhodamine labeling the water and bilayers, respectively. The relationship between the molecular composition and ordering inside the myelin figures and the surfactant structure has been investigated.

Introduction

During the swelling and dissolution of a surfactant lamellar (L_α) phase, different types of dynamic instabilities can be observed.[1] One such instability called "myelin figure" was first observed over 150 years ago by Virchow.[2] Since then, myelin figures have been formed using ionic surfactants including Aerosol OT (AOT),[3,4] nonionic surfactants including pentaethyleneglycol lauryl ether ($C_{12}E_5$),[5] triethyleneglycol lauryl ether ($C_{12}E_3$),[6] and phosphatidylcholine.[7,8] Myelin figures were also observed after the contact of oil with a surfactant aqueous solution.[9,10] On the basis of scanning electron microscopy observations of dehydrated samples,[7,11] myelin figures are considered to be tubular structures in which multiple surfactant bilayers are concentrically wrapped around a rodlike core of water. However, molecular organization, especially the distribution and orientation of water molecules inside the myelin figure, remains largely unknown. For a better understanding of the myelin figure formation mechanism and applications as a model system for myelin sheath, it is important to map myelin figures in their natural state using chemically selective imaging methods. Micro-Raman spectroscopy has recently been applied to probe the molecular conformation inside AOT myelin figures,[12] but the imaging speed and the spatial resolution of Raman microscopy[13] are not adequate for imaging a myelin figure with a growth rate of about 2 μm/s.[14]

The recently developed coherent anti-Stokes Raman scattering (CARS) microscopy [15,16] has been used for vibrational imaging of single bilayers,[17] live cells,[18−20] vesicles,[21−23] and live spinal tissues.[24] In CARS microscopy, a pump laser beam at frequency ω_p and a Stokes laser beam at frequency ω_s are tightly focused into a sample to generate an anti-Stokes signal at frequency $2\omega_p - \omega_s$.[25] The CARS intensity is significantly enhanced when $\omega_p - \omega_s$ is tuned to a Raman band, generating the vibrational contrast. The nonlinear dependence of the CARS signals on the excitation field intensity contributes to the 3D sectioning ability. It has been shown that the laser-scanning CARS microscopy has a lateral resolution of 0.3 μm and an axial resolution of 0.75 μm,[19] which is adequate

* Corresponding author. E-mail: jcheng@purdue.edu.

(1) Warren, P. B.; Buchanan, M. *Curr. Opin. Colloid Interface Sci.* **2001**, *6*, 287−293.
(2) Virchow, R. *Virchows Arch.* **1854**, *6*, 562.
(3) Buchanan, M.; Arrault, J.; Cates, M. E. *Langmuir* **1998**, *14*, 7371−7377.
(4) Haran, M.; Chowdhury, A.; Manohar, C.; Bellare, J. *Colloids Surf., A* **2002**, *205*, 21−30.
(5) Benton, W. J.; Raney, K. H.; Miller, C. A. *J. Colloid Interface Sci.* **1985**, *110*, 363−388.
(6) Buchanan, M.; Egelhaaf, S. U.; Cates, M. E. *Langmuir* **2000**, *16*, 3718−3726.
(7) Sakurai, I.; Suzuki, T.; Sakurai, S. *Biochim. Biophys. Acta* **1989**, *985*, 101−105.
(8) Harbich, W.; Helfrich, W. *Chem. Phys. Lipids* **1984**, *36*, 39−63.
(9) Lim, J. C.; Miller, C. A. *Langmuir* **1991**, *7*, 2021−2027.
(10) Mori, F.; Lim, J. C.; Raney, O. G.; Elsik, C. M.; Miller, C. A. *Colloids Surf.* **1989**, *40*, 323.
(11) Chapman, D.; Fluck, D. J. *J. Cell Biol.* **1966**, *30*, 1−11.
(12) Arunagirinathan, M. A.; Roy, M.; Dua, A. K.; Manohar, C.; Bellare, J. R. *Langmuir* **2004**, *20*, 4816−4822.
(13) Turrell, G., Corset, J., Eds. *Raman Microscopy: Development and Applications*; Academic Press, Inc.: San Diego, 1996.
(14) Mishima, K.; Yoshiyama, K. *Biochim. Biophys. Acta* **1987**, *904*, 149−153.
(15) Zumbusch, A.; Holtom, G. R.; Xie, X. S. *Phys. Rev. Lett.* **1999**, *82*, 4142−4145.
(16) Cheng, J. X.; Xie, X. S. *J. Phys. Chem. B* **2004**, *108*, 827−840.
(17) Potma, E. O.; Xie, X. S. *J. Raman Spectrosc.* **2003**, *34*, 642−650.
(18) Potma, E. O.; Boeij, W. P. D.; Haastert, P. J. M. v.; Wiersma, D. A. *Proc. Natl. Acad. Sci. U.S.A.* **2001**, *98*, 1577−1582.
(19) Cheng, J. X.; Jia, Y. K.; Zheng, G.; Xie, X. S. *Biophys. J.* **2002**, *83*, 502−509.
(20) Nan, X.; Cheng, J. X.; Xie, X. S. *J. Lipid Res.* **2003**, *40*, 2202−2208.
(21) Müller, M.; Schins, J. M. *J. Phys. Chem. B* **2002**, *106*, 3715−3723.
(22) Cheng, J. X.; Volkmer, A.; Book, L. D.; Xie, X. S. *J. Phys. Chem.* **2002**, *106*, 8493−8498.
(23) Cheng, J. X.; Pautot, S.; Weitz, D. A.; Xie, X. S. *Proc. Natl. Acad. Sci. U.S.A.* **2003**, *100*, 9826−9830.
(24) Wang, H.; Fu, Y.; Shi, R.; Cheng, J. X. *Biophys. J.* **2005**, *89*. In press.
(25) Levenson, M. D.; Kano, S. S. *Introduction to Nonlinear Laser Spectroscopy*; Academic Press: San Diego, 1988.

10.1021/la046820x CCC: $30.25
Published on Web 06/02/2005

for imaging the myelin figure. The molecular oscillators in a CARS process are stimulated to vibrate in phase when the beating frequency, $\omega_p - \omega_s$, is tuned to a Raman band. In the forward direction, the constructive interference of the CARS fields results in a highly directional signal that is proportional to n^2 with n being the number oscillators.[26] With a NA = 1.2 water objective, the collection efficiency for the Raman scattering is about 0.23, while the collection efficiency of an air condenser can be nearly 1.0 for the highly directional CARS singal.[19] The large signal and high collection efficiency lead to a high acquisition speed (~1 frame per second).[19] These capabilities allow us to map the molecular composition inside a 3D dynamic structure such as the myelin figures.

In this paper, we analyze the molecular composition and orientation inside the myelin figures using CARS and confocal fluorescence microscopy. Myelin figures were formed by contacting water with various surfactants including $C_{12}E_3$, AOT, and lecithin. The resonant CARS signals from the CH_2 and H_2O stretch vibration were used for selective imaging of the surfactant and water, respectively. Moreover, the polarization sensitivity of CARS was utilized to analyze the molecular orientation. We have acquired CARS images of uncoiled and helical myelin figures. Our results show that the concentric packing of surfactant bilayers inside the myelin figures highly depends on the molecular properties of the surfactant.

Materials and Methods

Materials. $C_{12}E_3$, lecithin dissolved in chloroform, and AOT were purchased from Sigma Chemical Co., U.S.A., with 99% chemical purity and used without further purification. The Tris powder was obtained from J.T. Baker Inc., U.S.A. Fluorescein isothiocyanate (FITC) was purchased from Molecular Probes. 1,2-Dioleoyl-*sn*-glycero-3-phosphoethanolamine-*N*-lissamine rhodamine B sulfonyl (DOPE−rhodamine) was purchased from Avanti Lipids.

Preparation of Myelin Figures. The penetration scan method [6] was used to prepare horizontally oriented myelin figures between two clean glass coverslips separated by an 80-μm spacer (Figure 1A). To form the $C_{12}E_3$ myelin figure, we brought distilled water and the pure surfactant into contact by capillary force. To form the lecithin myelin figure, we first made a film of lecithin on a coverslip and then used a 50 mM Tris buffer (pH = 7.5) containing 100 mM NaCl to swell the lipid film. The myelin figures of AOT were grown at the interface of the polycrystalline (powder) lamellar phase of AOT and the Tris buffer mentioned previously. To prepare vertically orientated myelin figures, we first made a chamber by attaching a silicone spacer with a hole of 10-mm diameter to a cover slip. A thin layer of $C_{12}E_3$ was placed on the bottom of the chamber, and then a drop of water was gently brought into contact with the $C_{12}E_3$ layer. All the myelin figures were prepared and imaged at 21 °C.

CARS Microscopy. A schematic of our CARS microscope is shown in Figure 1B. The 2.5-ps pump and Stokes beams were generated from two tightly synchronized Ti:sapphire oscillators (Coherent Inc, Mira900). The two excitation beams were collinearly combined. A Pockels cell (Conoptics, no. 350-160) was used to lower the repetition rate from 77 to 7.7 MHz, which reduces the average excitation power but maintains the peak power. The polarization direction of the parallel-polarized excitation beams was controlled by a half wave plate. After that, the beams were directed into a laser scanning microscope (Olympus Inc, FV300/IX70). A water immersion objective (NA = 1.2) was used to focus the laser beam into the sample. The CARS signal was collected in the forward direction using an air condenser (NA = 0.55) and detected with a photomultiplier tube (Hamamatsu, R3896). It is important to note that the collected signal is a coherent addition of nonresonant and resonant contributions.[27]

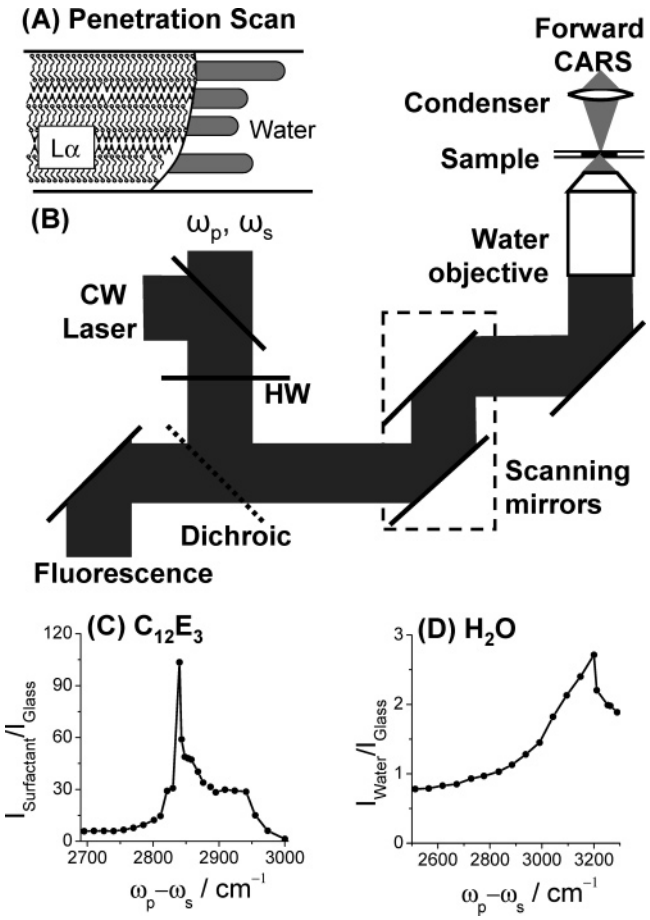

Figure 1. (A) Formation of myelin figures between two glass coverslips separated by a spacer of 80 μm. The lamellar phase is formed upon the contact of water or buffer with a film of lecithin, pure $C_{12}E_3$, or a polycrystalline powder of AOT. (B) Schematic of the CARS microscope. ω_p and ω_s are the frequencies of the pump and Stokes pulses, respectively. HW is the half-wave plate that controls the polarization of the excitation beams. The forward CARS signal is collected with an air condenser of 0.55 NA and detected with a photomultiplier tube (PMT). The two-color epifluorescence is excited by a 488-nm Ar^+ laser and is confocally detected by two independent PMTs. (C−D) CARS spectra of $C_{12}E_3$ and bulk water, respectively. The peak at 2840 cm^{-1} is from the symmetric CH_2 vibration in $C_{12}E_3$. The peak at 3200 cm^{-1} is from the symmetric H_2O vibration in water.

To identify the optimal wavelength for CARS imaging, we recorded the CARS spectrum of pure water and $C_{12}E_3$ liquid. We acquired a series of XZ images at different Raman shifts. Each XZ image contains a $C_{12}E_3$ or water area and a coverslip area. Each point in the spectra was obtained from the average CARS intensity from the $C_{12}E_3$ or the water area normalized by the average nonresonant CARS intensity from the coverslip area.

The polarization sensitivity of CARS was used to characterize the orientation of the CH_2 vibrational groups and the water molecules inside the myelin figure. The symmetric CH_2 stretch vibration in lipids gives a strong CARS signal.[22] The Raman scattering from liquid water is mainly contributed by the symmetric H_2O stretch vibrational mode.[28] For the symmetric vibration, when the excitation polarization is parallel with or perpendicular to the symmetry axis of CH_2 and H_2O, the resonant CARS field is contributed by the α_{11} or α_{33} component of the Raman tensor, respectively. Because α_{11} is much larger than α_{33}, the CARS signal is maximized when the dipole of CH_2 or H_2O

(26) Cheng, J. X.; Volkmer, A.; Xie, X. S. *J. Opt. Soc. Am. B* **2002**, *19*, 1363−1375.

(27) Shen, Y. R. *The Principles of Nonlinear Optics*; John Wiley and Sons Inc.: New York, 1984.

(28) Carey, D. M.; Korenowski, G. M. *J. Chem. Phys.* **1998**, *108*, 2669−2675.

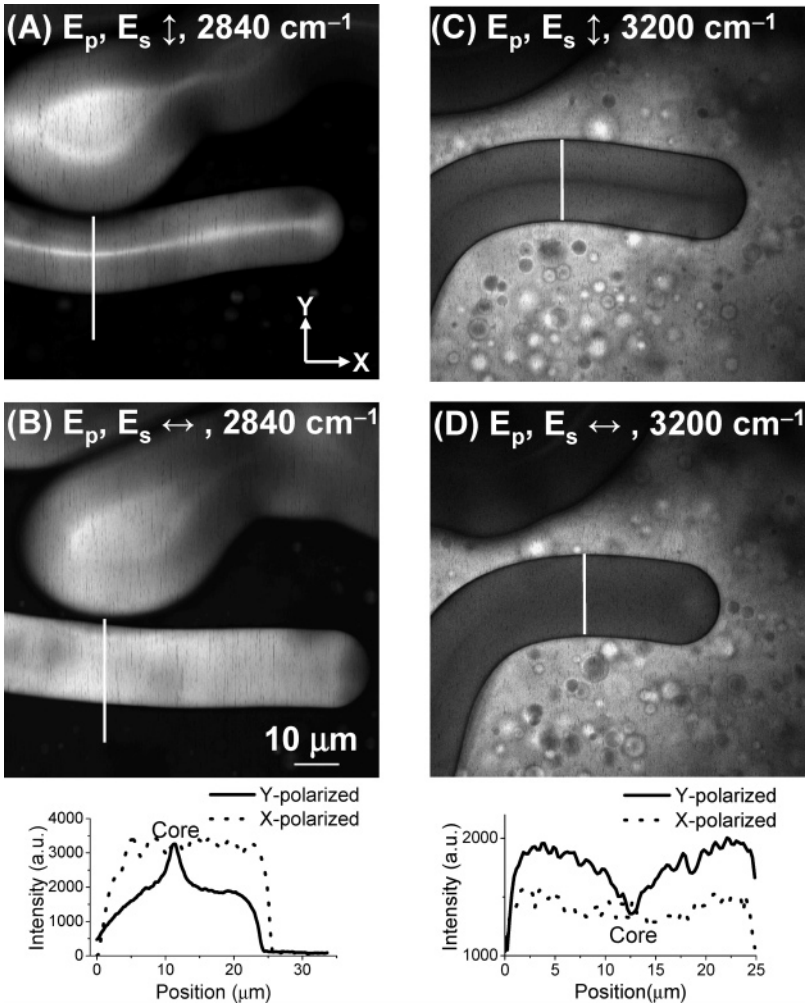

Figure 2. CARS images of $C_{12}E_3$ myelin figures. $\omega_p - \omega_s$ was tuned to 2840 cm^{-1} for CH_2 (A and B) and 3200 cm^{-1} for H_2O (C and D). The polarization direction of the parallel-polarized pump and Stokes beams is marked in each image. Shown below the images are the intensity profiles along the white lines in the images. The pump beam frequency was fixed at 14300 cm^{-1}. The average power of the pump and Stokes beam at the sample was 4.5 and 2.1 mW, respectively. Similar powers were used for other CARS images. The acquisition time was 2.7 s for each CARS image of 512 × 512 pixels. Due to their dynamic nature, the myelin figure growth direction changed after 5 min, the time we used to tune $\omega_p - \omega_s$ to 3200 cm^{-1}. The upper myelin figure is an example of a tadpole.

is parallel with the excitation polarization, and minimized when the dipole is perpendicular to the excitation polarization. By acquiring two CARS images of the same sample with x and y polarized beams, one can determine the molecular orientation on the basis of the relationship between the CARS intensity and the excitation polarization. We notice that the reflectivity of the dichroic mirror depends on the incident beam polarization. We also acquired the CARS images of bare coverslip which only generates the nonresonant background. The nonresonant CARS intensity is independent of the excitation frequency and the molecular orientation. To rule out the dependence of the CARS signal on the setup, we have normalized the CARS images from the samples by the nonresonant CARS intensity from the coverslip. Although the tight focusing used in our experiment leads to partial loss of the excitation polarization.[29,30] it has been shown that the CARS signal from an isotropic sample is linearly polarized along the excitation polarization direction.[31] This is because CARS is a third-order nonlinear process, and thus, the depolarized part contributes little to the signal. Therefore, we would assume that excitation polarization at the focus is the same as the incident polarization.

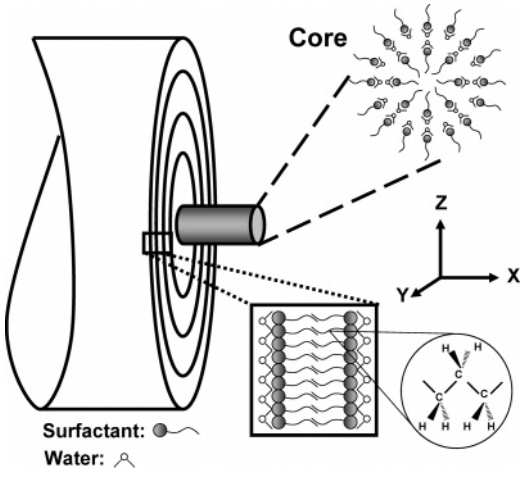

Figure 3. Illustration of the myelin figure structure based on our CARS data. The myelin figure is a tubular structure in which multiple surfactant bilayers are concentrically wrapped with partially ordered water molecules between adjacent bilayers.

Confocal Fluorescence Microscopy. For fluorescence imaging of myelin figures, we labeled the water phase with FITC

(29) Axelrod, D. *Biophys. J.* **1979**, *26*, 557−573.
(30) Koshioka, M.; Sasaki, K.; Masuhara, H. *Appl. Spectrosc.* **1995**, *2*, 224−228.
(31) Cheng, J. X.; Book, L. D.; Xie, X. S. *Opt. Lett.* **2001**, *26*, 1341−1343.

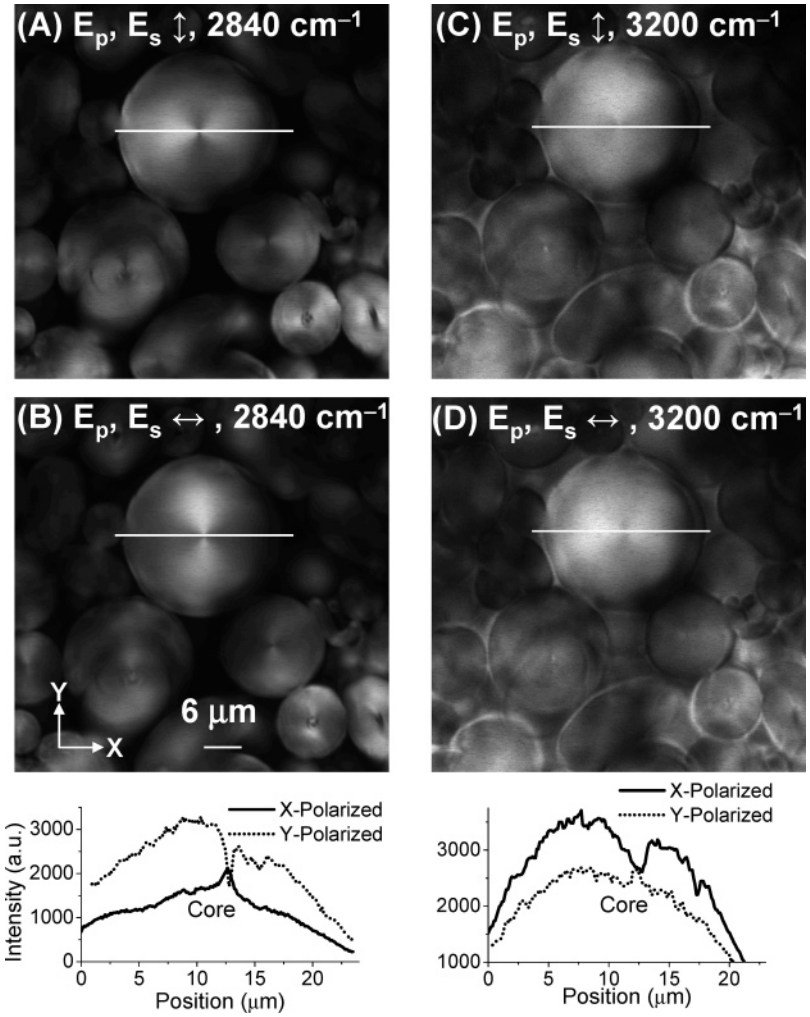

Figure 4. CARS images of the cross sections of $C_{12}E_3$ myelin figures. $\omega_p - \omega_s$ was tuned to 2840 cm^{-1} for CH_2 (A and B) and 3200 cm^{-1} for H_2O (C and D). The polarization direction of the parallel-polarized pump and Stokes beams is marked in each image. Shown below the images are the intensity profiles along the white lines in the images.

and the $C_{12}E_3$ surfactant phase with DOPE−rhodamine. A 488-nm Ar^+ laser was used to excite both FITC and DOPE−rhodamine. The signals from the two probes were spectrally separated and simultaneously detected with two photomultiplier tubes in the FV300/IX70 microscope.

All the images were analyzed using the FLUOVIEW software.

Results and Discussion

CARS Spectra of $C_{12}E_3$ and Water. The spectrum of $C_{12}E_3$ shown in Figure 1C displays a strong peak at 2840 cm^{-1} that arises from the symmetric CH_2 stretch vibration and a shoulder peak at 2860 cm^{-1} that arises from the asymmetric CH_2 stretch vibration. The broad shoulder band between 2900 and 3000 cm^{-1} is contributed by the CH_3 stretch vibration. The 2840 cm^{-1} band shows a signal-to-background ratio of 16.4, which is adequate for selective imaging of the surfactants including $C_{12}E_3$, AOT, and lecithin. The resonant CARS signal from water shown in Figure 1D is much weaker than that from $C_{12}E_3$. The CARS peak for the symmetric H_2O vibration is shifted to 3200 cm^{-1} because of the interference between the resonant and nonresonant CARS contributions.[27] The resonant CARS signal from water becomes negligible in the 2600−2900 cm^{-1} region where the CH_2 stretch vibration band resides.

CARS Images of Single Myelin Figures. We started with $C_{12}E_3$ because its equilibrium phase diagram is well-known.[32] Due to the large water miscibility gap of $C_{12}E_3$, the lamellar phase does not dissolve directly into the micellular phase. Instead the lamellar phase can coexist with the water phase. Thus, myelin figures can be formed with ease.[6] After the contact of $C_{12}E_3$ with water, we observed the growth of myelin figures at the L_α/water interface. On the basis of the spectra in Figure 1C,D, we tuned $\omega_p - \omega_s$ to 2840 and 3200 cm^{-1} for imaging $C_{12}E_3$ and water, respectively. We focused the laser beams into the equatorial plane of the myelin figure. Figure 2 shows the dependence of the CARS intensity from the myelin figures on the excitation polarization. A myelin "core" is clearly observed with the resonant CARS signal from $C_{12}E_3$ (Figure 2A) and water (Figure 2C). With the excitation fields polarized along either the *x* or the *y* direction, the core of the lower myelin figure gives a strong and polarization-independent CARS signal at 2840 cm^{-1} (Figure 2A,B), indicating the presence of the surfactant inside the core. For the CARS signal at 3200 cm^{-1}, the intensity profiles below Figure 2C,D show that the signal from the core is lower than that from the region outside of the core with *y*-polarized excitation and equal to the signal from the region outside of the core with *x*-polarized excitation. The water signal from the core is the same

(32) Mitchell, D. J.; Tiddy, G. J. T.; Waring, L.; Bostock, T.; McDonald, M. P. *J. Chem. Soc., Faraday Trans.* **1983**, *79*, 975.

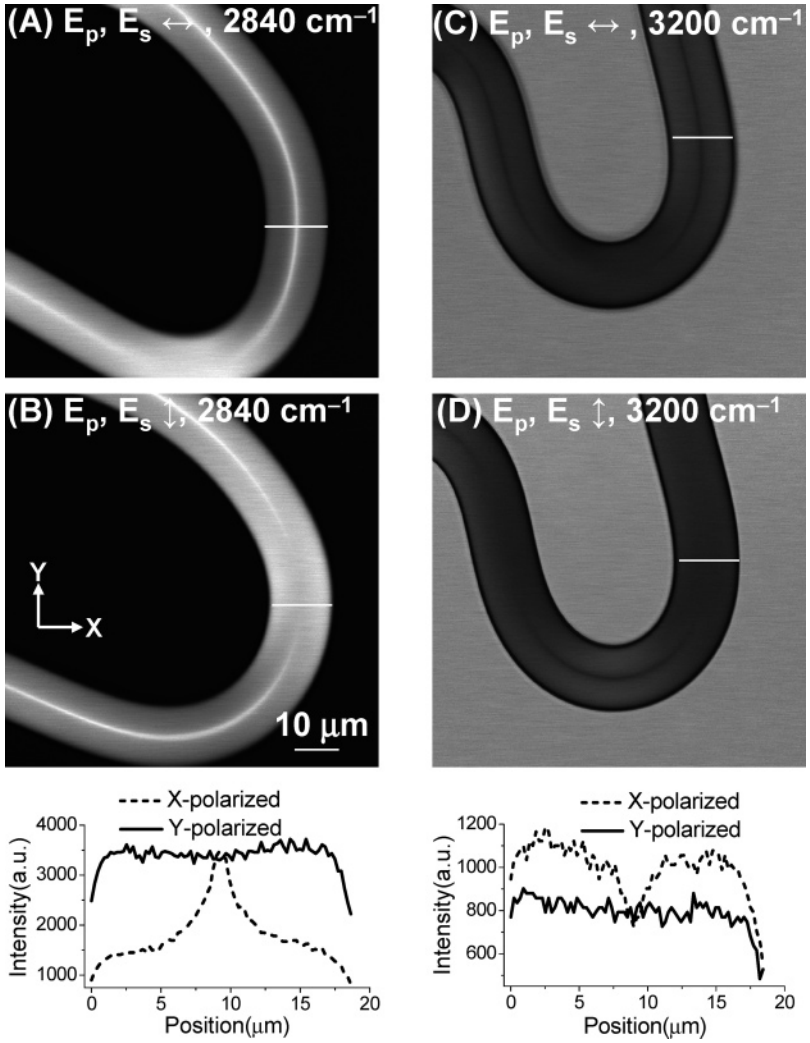

Figure 5. CARS images of lecithin myelin figures. $\omega_p - \omega_s$ was tuned to 2840 cm^{-1} for CH_2 (A and B) and 3200 cm^{-1} for H_2O (C and D). The polarization direction of the parallel-polarized pump and Stokes beams is marked in each image. Shown below the images are the intensity profiles along the white lines in the images.

with both *x*- or *y*-polarized excitation, as indicated by the intensity profiles below Figure 2D.

On the basis of the above observations, we propose a core structure illustrated in Figure 3. The $C_{12}E_3$ molecules form a cylindrical micelle in the center of the myelin figure. Because the longitudinal and axial widths of the excitation volume are 0.75 and 0.3 μm, respectively,[19] most of the signal is contributed by the molecules orientated along the *z* direction when the laser beams are focused in the center of the core area. For $C_{12}E_3$ molecules along the *z* direction, the CH_2 groups are uniformly oriented in the *x*−*y* plane. Therefore, the signal is independent of the excitation field polarization, as observed from the intensity profiles below Figure 2B. With *x*-polarized excitation, the water signal from the core is lower than that from the surrounding area, indicating that no sizable water core exists in the $C_{12}E_3$ myelin figures.

For the area surrounding the core, the CARS signal from the CH_2 vibration with *x*-polarized excitation is about 1.8 times stronger than that with *y*-polarized excitation. This indicates that the $C_{12}E_3$ molecules in the equatorial plane are orientated along the *y* direction (Figure 3). With $\omega_p - \omega_s$ tuned to 3200 cm^{-1}, the CARS intensity for water is stronger with *y*-polarized excitation (Figure 2C,D), opposite from the CARS intensity for $C_{12}E_3$. This proves that the interlamellar water is partially ordered, with the symmetry axis perpendicular to that of the CH_2 groups in $C_{12}E_3$.

The upper myelin figure in Figure 2 has a tadpole-shaped head of 10 μm in dimension. The CARS intensity from the center area of the tadpole displays little polarization dependence and is the same as that from the myelin core at CH_2 vibration. In addition, it is much lower than the CARS intensity from bulk water at H_2O vibration. These observations suggest that the tadpole is filled with an ordered structure in which the $C_{12}E_3$ molecules are ordered along the *z* direction. On the basis of the use of tracer particles that monitored the influx of water into the lamellar phase,[6] it was proposed that water enters the lamellar phase at the myelin roots and feeds the myelin figures which then grow into the water phase.[7] Such water backflow would result in a water-filled tadpole, which is, however, not observed in our experiment. Therefore, our result indicates there is no significant amount of water backflow along the core of the myelin during its growth.

The CARS signal from the tip of the lower myelin figure in Figure 2 displays a clear polarization dependence which indicates an onion-like multilamellar structure. A similar structure has been observed in a previous CARS imaging study of phospholipid onions.[23]

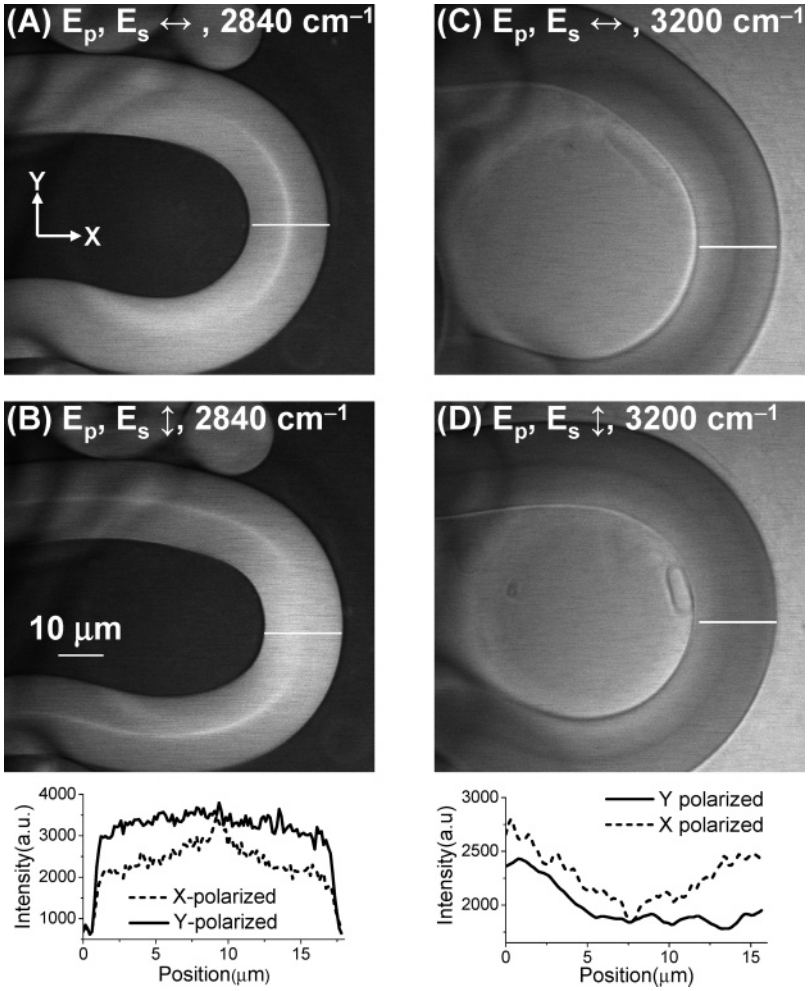

Figure 6. CARS images of AOT myelin figures. $\omega_p - \omega_s$ was tuned to 2840 cm^{-1} for CH_2 (A and B) and 3200 cm^{-1} for H_2O (C and D). The polarization direction of the parallel-polarized pump and Stokes beams is shown in each image. Notice the large CARS intensity from water in the myelin. Below the images are the intensity profiles along the white lines in the images.

From the intensity profiles shown in Figure 2, the full width at half-maximum of the core area is about 1.5 μm. This value is associated with the axial resolution of our setup. To provide a better resolution, we have studied the cross sections of the $C_{12}E_3$ myelin figures growing along the z axis. The CARS images shown in Figure 4 display a clear polarization dependence, which confirms the concentric bilayer structure and ordering of water inside the myelin figure. For either CH_2 or H_2O vibration, the CARS intensity signal from the center of the myelin figure is between the CARS intensities from the surrounding area the x- and y-polarized excitation, supporting a circularly symmetric orientation of the molecules in the core area. The smallest core width we have observed is 0.3 μm, coinciding with the lateral resolution of our setup. The intensity profiles below Figure 4D further suggest the absence of a sizable water core in the myelin figure, supporting the structure illustrated in Figure 3.

Besides $C_{12}E_3$, we have studied single, uncoiled myelin figures formed of lecithin and AOT. The results are shown in Figures 5 and 6, respectively. The CARS images show the same polarization independence as the $C_{12}E_3$ myelin figures for the CH_2 and H_2O vibration signals from both the core and the peripheral regions. The images in Figures 5C and 6C indicate the absence of a sizable water core, consistent with our data for $C_{12}E_3$ myelin figures. Because the AOT and lecithin molecules have two hydrocarbon chains, an inverse micelle might be formed in the center of the myelin figure.

The CARS images of different surfactants allow us to study the relationship between the molecular composition and organization inside the myelin figures and the properties of the surfactants used. The analysis is presented below.

Molecular Composition and Organization inside Myelin Figures. Using the CARS signal at 2840 cm^{-1}, we are able to quantify the packing density of the surfactant molecules using the value of $I_{\parallel}/I_B$, where I_B is the average CARS intensity from the bulk water at 2840 cm^{-1} and $I_{\parallel}$ is the average CARS intensity from the myelin figure with the excitation polarization parallel with the myelin length. Here the normalization with I_B rules out the variation of excitation powers at different experiments. The results are shown in Figure 7A. The myelin figures of lecithin that has two hydrocarbon chains give the highest packing density. This is consistent with our observation that the lecithin myelin figures are the most stable of the three. The AOT myelin figures have the lowest packing density possibly because AOT has two side chains linked to its short hydrocarbon chains. Using the same method, we have compared the water content inside the myelin figures. It is interesting that the trend of water content shown in Figure 7B is opposite to that of the surfactant packing density. The AOT myelin has the highest water content at a value of 0.88, which is 2.02 times that of lecithin and 1.52 times that of $C_{12}E_3$. This finding is consistent with the fact that the repulsion force

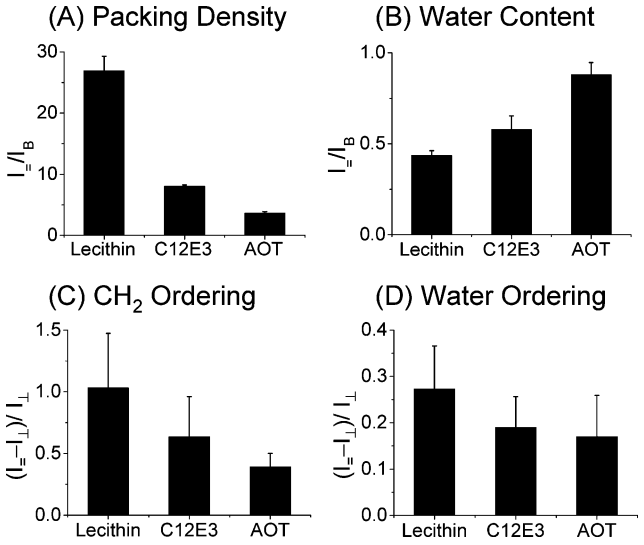

Figure 7. (A) and (B) Comparison of the CH_2 packing density and the water content in myelin figures formed of lecithin, $C_{12}E_3$, and AOT. (C) and (D) Comparison of the ordering degree of CH_2 and water in myelin figures formed of lecithin, $C_{12}E_3$, and AOT.

between charged surfactant bilayers is greater than that between nonionic surfactant bilayers.

As we have shown, the difference between the CARS intensities $I_{\parallel}$ and $I_{\perp}$ arises from molecular ordering. Here $I_{\parallel}$ and $I_{\perp}$ are the average CARS intensities from the myelin figure with the excitation polarization parallel with or perpendicular to the myelin length, respectively. The value of $(I_{\parallel} - I_{\perp})/I_{\perp}$ is used to estimate the ordering degree of the surfactant molecules and water inside the myelin. $(I_{\parallel} - I_{\perp})/I_{\perp}$ is zero for randomly orientated molecules.

For CH_2 groups, the ordering degree for lecithin myelin figures is 1.6 times that of $C_{12}E_3$ and 2.9 times that of AOT myelin figures (Figure 7C). The difference in ordering can be explained using the surfactant structure. Lecithin is a mixture of unsaturated lipids with two fatty acid side chains with 16−18 hydrocarbon groups. The long hydrocarbon chains prohibit and limit conformation change of the CH_2 groups in the concentric bilayers. $C_{12}E_3$ has a lower degree of ordering than lecithin because $C_{12}E_3$ only has one long hydrocarbon chain. AOT has the lowest degree of ordering primary due to its two short, branched hydrocarbon chains. Using micro-Raman spectroscopy, Arunagirinathan et al. have shown that AOT myelins have a mixture of both gauche conformers and trans conformers.[12] Our visualization of the low CH_2 ordering degree in AOT myelin figures is in agreement with their spectroscopic measurement.

The degree of water ordering in various surfactant myelin figures followed a trend similar to that of the CH_2 degree of ordering. As shown in Figure 6D, the ordering degree of water for lecithin, $C_{12}E_3$, and AOT myelin was 0.27, 0.19, and 0.17, respectively. The difference in the degree of ordering for water is related to the water content in the myelin and is dependent on the polar headgroup of the surfactant. For lecithin myelin figures that have less water inside, the chance of water molecules associating with the headgroup of lecithin could be greater. As a result, the water in the lecithin myelins appears to be more ordered. The AOT myelin figures have much higher water content than $C_{12}E_3$, but their degrees of water ordering are similar. It is likely that the negative charge in AOT increases the bilayer potential and thus increases the number of ordered water molecules. We note that water

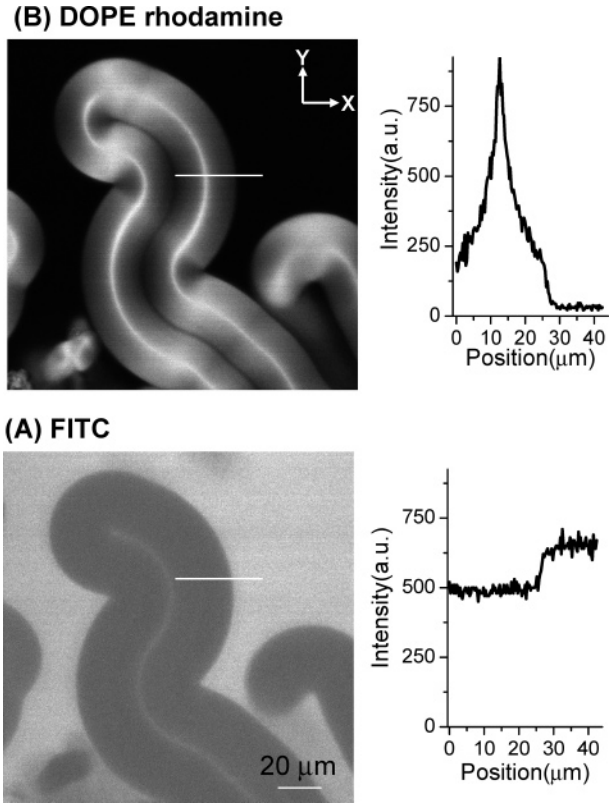

Figure 8. Confocal fluorescence images of $C_{12}E_3$ myelin figures. (A) Signal from DOPE−rhodamine that labels the surfactant bilayers. (B) Signal from FITC that labels the water phase. The intensity profiles along the white lines are shown to the right.

ordering between two lipid bilayers has been studied by different experimental and theoretical methods,[33−35] but it is unclear whether the hydration water is oriented by the electric field or by the constraints of hydrogen bonds.[36] The myelin figures formed of various surfactants provide a unique system to the study of structured water at the biological interface. As shown here, the water is partially ordered even when a neutral surfactant $C_{12}E_3$ is used, indicating the role of hydrogen-bonding interaction in water ordering.

Confocal Fluorescence Imaging. Although the CARS signals are directly from the surfactant and water molecules, we should point out that water is a weak Raman scatterer as shown in Figure 1D. We might not be able to detect a water core with a diameter smaller than the lateral resolution of CARS microscopy. A water-soluble dye would help us to map the 3D water distribution inside the myelin figure with a much higher sensitivity. We have carried out confocal fluorescence imaging of lecithin myelin figures using the signal from FITC that labels the water phase and DOPE−rhodamine that is incorporated into the lecithin bilayers. The results are shown in Figure 8. We observed a strong red fluorescence signal of DOPE−rhodamine from the core area with the *x*-polarized excitation field. The core fluorescence intensity from the *y*-oriented segments is the same as that from the *x*-oriented segments. The dipole in DOPE−rhodamine is perpen-

(33) McIntosh, T. J.; Simon, S. A. *Annu. Rev. Biophys. Biomol. Struct.* **1994**, *23*, 27−51.
(34) Marrink, S. J.; Berkowitz, M. In *Permeability and Stability of Lipid Bilayers*; Disalvo, E. A., Simon, S. A., Eds.; CRC Press: Boca Raton, 1995.
(35) Leikin, S.; Parsegian, V. A.; Rau, D. C.; Rand, R. P. *Annu. Rev. Phys. Chem.* **1993**, *44*, 369−395.
(36) Gawrisch, K.; Ruston, D.; Zimmerberg, J.; Parsegian, V. A.; Rand, R. P.; Fuller, N. *Biophys. J.* **1992**, *61*, 1213−1223.

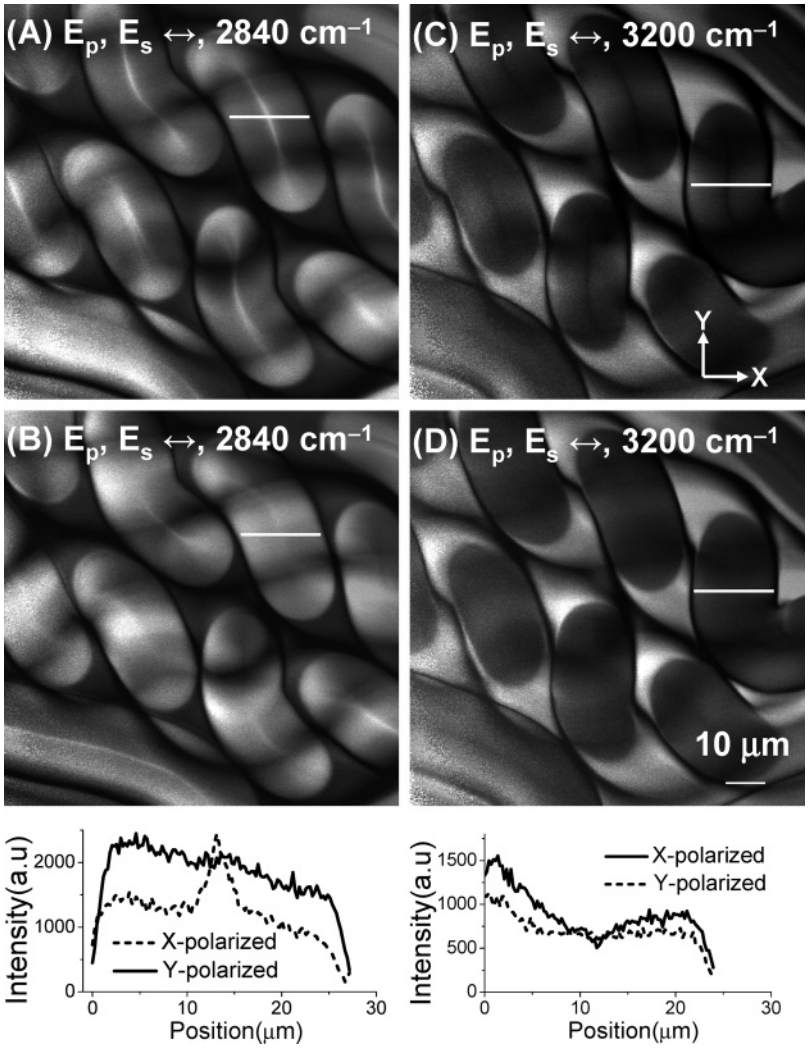

Figure 9. CARS images of a double helix structure of lecithin myelin figures. $\omega_p - \omega_s$ was tuned to the CH_2 vibration at 2840 cm^{-1} and the H_2O vibration at 3200 cm^{-1}, respectively. The polarization direction of the parallel-polarized pump and Stokes beams is marked in each image. Shown below the images are the intensity profiles along the white lines in the images.

dicular to the hydrocarbon chains of the probe and shares the same orientation as the CH_2 groups in the lecithin molecules. Thus, the polarization independence of the fluorescence signal indicates that the surfactant molecules are orientated along the *z* direction, in agreement with the CARS data. The distribution of FITC is shown in Figure 8B. We observed a stronger green fluorescence signal from the bulk water phase and a weaker signal from the myelin figures. There was not a detectable increase of fluorescence from the core area. This result confirms that there not a sizable water core in the myelin figure.

Helical Myelin Figures. Besides single uncoiled myelin figures, the double helix structure of myelin figures has been previously reported.[37−39] The helix structure is thermodynamically a consequence of myelin figure winding to minimize the sum of the intermembrane binding energy and the membrane bending elastic energy.[38] It is known that lecithin commonly forms helical myelin figures.[37,38] The CARS images of two double helical myelin figures are shown Figure 9. We find that the CARS signal from the myelin core is independent of the excitation polarization. The ordering degree of CH_2 groups is measured to be 0.60, lower than that of the uncoiled lecithin myelin figures possibly due to the twisting. Another interesting phenomenon we have observed is the asymmetric water distribution along the cross section of the myelin figure, as shown in the intensity profiles below Figures 9D and 6D. The lateral resolution and the axial resolution of CARS microscopy are about 0.3 and 0.75 μm, respectively,[19] much smaller than the myelin diameter. Thus, the CARS signal gradient reflects the change in water concentration across the myelin figure. Such asymmetric water distribution is likely a consequence of the bending of myelin figures.

Conclusions

We have mapped the molecular composition and orientation inside the myelin figures of $C_{12}E_3$, AOT, and lecithin using the resonant CARS signal from CH_2 and H_2O stretch vibrations. Combining the molecular selectivity and polarization sensitivity of CARS, we have shown that the myelin figures are composed of concentric bilayers of surfactant with partially ordered water layers residing between adjacent bilayers. No sizable water cores or water-filled tadpoles are observed inside the myelin figures. The CARS data was confirmed by confocal fluorescence

(37) Lin, K. C.; Weis, R. M.; McConnell, H. M. *Nature* **1982**, *296*, 164−165.
(38) Mishima, K.; Fukuda, K.; Suzuki, K. *Biochim. Biophys. Acta* **1992**, *1108*, 115−118.
(39) Frette, V.; Tsafrir, I.; Guedeau-Boudevile, M.; Jullien, L.; Kandel, D.; Stavans, J. *Phys. Rev. Lett.* **1999**, *83*, 2465−2468.

microscopy with FITC and DOPE−rhodamine labeling the water and bilayers, respectively. The relative composition and ordering degree of the molecules inside the myelin figures is found to be highly dependent on the molecular properties of the surfactant used. With the advantages of chemical bond selectivity, high imaging speed, 3D spatial resolution, large penetration depth, and polarization sensitivity, CARS microscopy opens up a new approach to characterizing various dynamic 3D structures, as shown in this work.

Acknowledgment is made to the donors of the American Chemical Society Petroleum Research Fund (no. 41741-G7) for support of this research. We thank Haifeng Wang for his help in the CARS imaging experiments.

LA046820X